Sensors and Materials, Vol. 38, No. 1 (2026) 149–161
MYU Tokyo

S & M 4291

Fundamental Study on Inhibiting Factors of Self-propagating Exothermic Reaction of Al/Ni Multilayer Powders: Effects of Pre-annealing

Souto Yamashita,[1*] Kousuke Ito,[2] and Shugo Miyake[1,2]

[1]Division of Innovation and Creativity Engineering, Graduate School of Science and Engineering, Setsunan University,
17-8 Ikeda-Nakamachi, Neyagawa, Osaka 572-8508, Japan
[2]Department of Mechanical Engineering, Faculty of Science and Engineering, Setsunan University,
17-8 Ikeda-Nakamachi, Neyagawa, Osaka 572-8508, Japan

(Received October 30, 2025; accepted November 27, 2025)

Keywords: Al/Ni multilayer powders, exothermic reaction characteristics, heat treatment, thermal transport, microstructure

In this study, Al/Ni multilayer powders fabricated by cold rolling were subjected to heat treatment to investigate the effects of the change in microstructure on their exothermic reaction characteristics. Heat treatment at 180 °C for 48 h caused only minor crystallite growth but significantly delayed the self-propagating exothermic reaction, suggesting that the expansion of the Al/Ni interfacial mixing layer reduced the diffusion driving force and reaction rate. Thermoreflectance (TR) measurements of powder cross sections revealed that Ni regions acted as local thermal barriers in low-pass powders, while 40-pass powders exhibited uniform phase lag distributions, indicating an improved continuity of thermal transport pathways. These findings demonstrate that the exothermic characteristics of Al/Ni multilayer powders are governed not only by crystallite size but also by nanoscale interface structure and local thermal transport uniformity. The results newly clarify that reaction retardation under heat treatment cannot be explained solely by grain growth but is strongly associated with the expansion of interfacial mixing layers and the deterioration of heat transport.

1. Introduction

The rapid proliferation of electronic devices in modern society, driven by demands for environmental sustainability and user safety, has brought about remarkable advancements in electronic control technologies. Electronic control units have been increasingly integrated into components and products that previously lacked control systems, greatly enhancing both functionality and reliability. At the same time, the technologies that enable these devices are required to meet increasingly stringent standards for performance and reliability. Among the

*Corresponding author: e-mail: 2552d101ys@edu.setsunan.ac.jp
https://doi.org/10.18494/SAM5996

ISSN 0914-4935

essential processes in electronics manufacturing, the conventional reflow soldering process remains indispensable; however, it inevitably involves prolonged heating and infrared irradiation, leading to problems such as the thermal degradation of sensitive components, the warping of substrates, and joint defects. These issues underscore the growing need for alternative joining techniques that can achieve strong interfacial bonding while minimizing thermal exposure.

One promising solution is the localized heating technique based on the self-propagating exothermic reaction (SPER) in aluminum (Al)/nickel (Ni) multilayer systems.[1–17] Al/Ni multilayer materials, as their name suggests, are characterized by a multilayer structure formed by extremely thin Al and Ni layers. When adjacent Al and Ni layers receive minute energy from a heat source such as a spark, atomic diffusion occurs, severing the Al–Al and Ni–Ni bonds. This leads to the formation of Ni–Al intermetallic compounds with diverse compositions. The amount of energy released during this reaction varies depending on the type of intermetallic compound formed. However, as shown in the following equation, when transitioning from Ni–Ni or Al–Al bonds to Ni–Al bonds, the difference in bond energy is released as heat.

$$\Delta H = H_{\mathrm{Ni-Al}} - \left(H_{\mathrm{Al}}, H_{\mathrm{Ni}}\right) \tag{1}$$

Among Ni–Al intermetallic compounds, NiAl is cited as a representative example. When atomic diffusion occurs upon the application of a small amount of energy, Ni and Al with face-centered cubic (fcc) structures bond to form NiAl with a CsCl-type bcc structure. Their difference in bond energy is released as heat. The released energy induces the following reaction, causing the exothermic reaction to propagate spontaneously. When NiAl forms from Al and Ni, the formation enthalpy is -60–70 kJ/mol.[18–22] The formation enthalpy of NiAl is the highest among Ni–Al intermetallic compounds. Therefore, to maximize the exothermic reaction characteristics, Ni and Al must react in a 1:1 ratio by the number of atoms. Al/Ni multilayer materials have been fabricated in various forms, such as cold-rolled powders and magnetron-sputtered multilayer films. Previous studies have revealed correlations between the fabrication method, the resulting microstructure, and exothermic properties, suggesting their potential for use in advanced joining applications.

In our previous studies on Al/Ni multilayer powders fabricated by cold rolling and pulverizing, we demonstrated that increasing the number of rolling cycles refines the multilayer structure, reduces the number of unreacted Al and Ni regions, and enhances both the maximum calorific value and the heat propagation rate, thereby clarifying the role of macroscopic structural refinement in improving exothermic properties.[5–8,17] However, since the self-propagating exothermic reaction proceeds through nanoscale instantaneous reactions, it appears as intermittent propagation on the macroscopic scale. Therefore, understanding the exothermic behavior of Al/Ni multilayers requires the consideration of heat transport at the nanoscale. In Al/Ni multilayer films, for example, nanoscale Ni–Al interfacial mixing layers have been identified as a key factor contributing to the discrepancy between the measured and theoretical total calorific values. Similarly, in multilayer powders, the crystallite growth of several tens of nanometers has been associated with enhanced heat propagation. The mass per mole of the NiAl

compound, calculated from the atomic masses of Al and Ni, is 42.84 g/mol. Experimental results show that both multilayer powders and films exhibit total calorific values slightly smaller than the theoretical value (the mass per mole of the NiAl compound, calculated from the atomic masses of Al and Ni, is 42.84 g/mol, and the heat of formation per gram is estimated to be 1634 J/g); for instance, sputtered Al/Ni films with a bilayer thickness of 100 nm and a total thickness of 30 μm exhibited 1617 J/g, which is comparable to that of 40-pass rolled powders.[17] Although this deviation was initially attributed to unreacted regions in the powders, synchrotron radiation experiments revealed complete transformation into NiAl and confirmed crystallite growth with increasing number of rolling cycles, suggesting that nanoscale structural factors such as crystallite size and interfacial mixing, rather than incomplete reactions, govern the deviation from theoretical values and the enhancement of exothermic behavior in Al/Ni multilayer systems.

Considering the above findings, and given that the total calorific values of multilayer powders and films are comparable, it is reasonable to infer that similar interfacial mixing layers may also contribute to the deviation between the theoretical and measured calorific values in multilayer powders. Furthermore, considering microstructure and bilayer thickness, the following equation has been proposed for the heat propagation velocity in multilayer materials:

$$v_x^2 = \left(\sum_{n=odd} \frac{k_n}{a_n^3} \right)^{-1} \frac{\lambda^2 R T_{max}^2}{E\left(T_a - T_0\right)} A d' \exp\left(-E / R T_{max}\right). \tag{2}$$

Equation (2), developed by Gavens *et al.*,[23] is based on the heat conduction equation and accounts for the effects of atomic diffusion within the interfacial mixing layer of multilayer materials. The symbols used in Eq. (2) are defined as follows: v_x is the reaction propagation velocity; k_n and a_n are the Fourier expansion coefficients and eigenvalues, which depend on the interfacial composition profile; λ is the thermal diffusivity; R is the gas constant; T_{max} is the maximum temperature during the reaction; T_a is the ideal adiabatic temperature assuming no intermixing or heat loss; T_0 is the initial temperature; A is the Arrhenius pre-exponential factor for diffusion; E is the diffusion activation energy; and $d'=d/4$ represents one-quarter of the bilayer thickness d (the combined thickness of the Al and Ni layers). This equation, which extends the Armstrong and Koszykowski model,[24] incorporates the effect of the intermixed interfacial region on the reaction rate. As the interfacial mixing layer becomes thicker, the released energy and the maximum temperature T_{max} decrease, resulting in a reduction in the reaction velocity v_x. Therefore, Eq. (2) implies that, in addition to the effect of atomic diffusion associated with the microstructure, changes in thermal conductivity properties caused by cold rolling must also be considered.

Considering these findings, it remains unclear how microstructural factors—including crystallite size, interfacial mixing layers, and rolling-induced structural changes—systematically affect the exothermic reaction characteristics and nanoscale heat transport in Al/Ni multilayer powders. Therefore, the objective of this study is to clarify these relationships by analyzing powders subjected to different numbers of rolling cycles by X-ray diffraction, calorimetry, and

thermoreflectance measurements. This approach allows a comprehensive evaluation of the interplay between microstructure, thermal transport, and reaction propagation. In this study, we systematically investigated how microstructural factors—such as crystallite size and microstructural changes induced by cold rolling—affect the exothermic reaction characteristics of Al/Ni multilayer powders. To clarify these effects, cold-rolled powders were subjected to low-temperature annealing at 180 °C for 48 h followed by air cooling to modify their grain size and internal structure, and the resulting changes in heat generation behavior were examined. Furthermore, considering that atomic diffusion and microstructural evolution during cold rolling can alter thermal conductivity, the thermoreflectance (TR) method was employed to visualize nanoscale heat transport in powders subjected to different numbers of rolling cycles, and the effects of cold rolling on both thermal transport and exothermic properties through changes in microstructure and thermal conductivity were comprehensively evaluated.

2. Experiments

2.1 Al/Ni multilayer powder and heat treatment

Al/Ni multilayer powders were fabricated by cold rolling and frictional pulverization. Commercially available pure aluminum (>99.5%) and pure nickel (>99.9%) foils were prepared and cut into pieces approximately 54 × 54 mm^2 in size. From their atomic ratio and density, the required thicknesses of the aluminum and nickel foils were calculated to be 0.030 and 0.020 mm, respectively, for effective interaction, and the foils were alternately stacked. The Al/Ni multilayer foils, with a total mass of approximately 1 g, were cold-rolled into metal strips (100 × 100 × 1 mm^3) to be used as sacrificial materials. The rolling gap was set to 2.3, corresponding to the rolling condition for samples subjected to 40 passes in a previous study. After initial cold rolling, the foils were folded in half and further rolled to prepare samples subjected to 10, 20, 30, and 40 passes (these numbers were arbitrarily selected). After rolling, the samples were pulverized in a mill. The resulting powders were classified using sieves with mesh sizes of 75 and 250 μm; in accordance with the Japanese Industrial Standard, only particles within the 75–250 μm range were collected. The sample preparation conditions were consistent with those reported previously.[5–8]

As shown in Fig. 1, the observed macroscale structure reveals that the SEM cross section of the 20-pass rolled powder exhibits an inhomogeneous morphology and discontinuous reaction interfaces, reflecting the limited number of rolling cycles and indicating unstable reaction propagation. In contrast, the SEM cross section of the 40-pass rolled powder shows a uniform structure with continuous reaction interfaces, suggesting that the reaction proceeds more stably. Consequently, variability is considered to have been reduced. Here, the "uniformity of structure" being defined is determined by whether the exothermic reaction occurs continuously and completely. Specifically, in the 20-pass powder, the Al and Ni layers remain tens of micrometers thick, whereas in the 40-pass powder, they are reduced to only a few micrometers. Previous studies[5–8] report that such thin layers in the 40-pass powder enable a sufficiently uniform exothermic reaction, leaving no residual pure Al or Ni after heating, as confirmed by X-ray

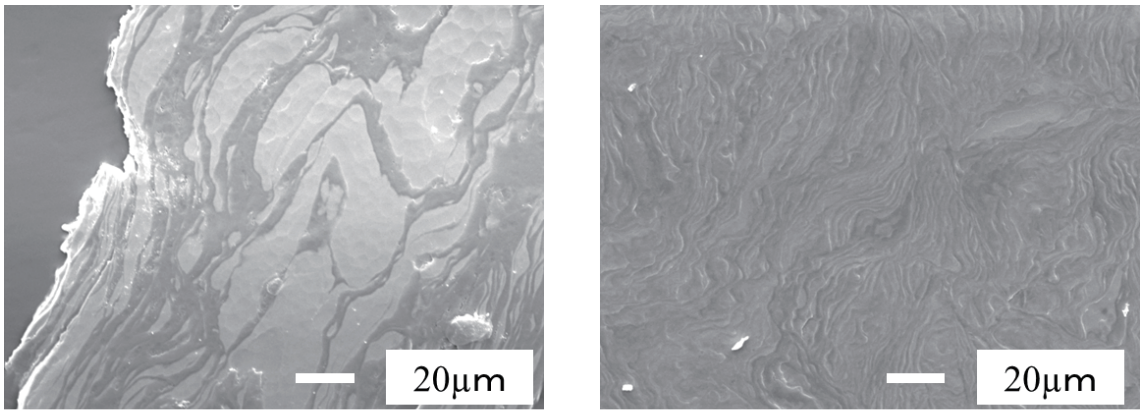

Fig. 1. SEM cross-sectional views of Al/Ni multilayer powder material: (a) 20 and (b) 40 passes.

analysis. In contrast, residual Ni is observed in the 20-pass powder. Therefore, we consider the 20-pass powder to have a non-uniform cross section, while the 40-pass powder is regarded as uniform.

Taking the temperature conditions reported to induce crystallite recovery in high-purity aluminum[25] and the low-temperature annealing conditions known[23] to promote the growth of Ni–Al nanoscale mixing layers in multilayer films, the rolled multilayer powders were subjected to heat treatment at 180 °C for 48 h, followed by air cooling. The crystallite size was analyzed by the Halder–Wagner method using X-ray diffraction (XRD) profiles.

2.2 Determination of crystallite size

The crystallite size analysis method employed the Halder–Wagner method using X-ray diffraction (XRD) profiles measured by powder X-ray diffraction (MiniFlex600, Rigaku). The Scherrer equation, commonly used for analyzing typical crystallite size, is expressed as Eq. (3) below. K is called the Scherrer constant, which is determined by the shape of the crystallite. $(\delta_{2\theta})_D$ is the broadening of the diffraction peak profile owing to lattice distortion, and $(\delta_{2\theta})_S$ is the broadening of the diffraction peak profile owing to the crystallite size D.

$$(\delta_{2\theta})_D = 4e\tan\theta \tag{3}$$

$$(\delta_{2\theta})_S = \frac{K\lambda}{D\cos\theta} \tag{4}$$

Equations (3) and (4) express the broadening of the diffraction peak profile as a function of the lattice distortion e and crystallite size D, respectively. The diffraction peak profile, characterized by small crystallite size and lattice distortion, is the convolution of profiles arising from these two factors. Therefore, to separate the profiles on the basis of each factor, it is necessary to

assume the shape of each profile. The Halder–Wagner method is used to determine the crystallite size and lattice strain.[26,27] According to Halder and Wagner, the integral width of the Lorentz function represents the crystallite size B_C.[27] On the other hand, the integral width of the diffraction peak profile due to lattice distortion is assumed to be represented by a Gaussian function B_G. It was proposed that the following approximate relationship holds between the integral width B of the profile formed by convolving these functions:

$$\frac{B_C}{B} = 1 - \left(\frac{B_G}{B}\right)^2. \tag{5}$$

Here, the profile spread is represented by the integral width, and since $B_C = \left(\delta_{2\theta}\right)_D$ and $B_G = \left(\delta_{2\theta}\right)_S$, Eq. (5) can be expressed as Eq. (6) based on Eqs. (3) and (4).

$$\frac{K\lambda}{\beta D\cos\theta} = 1 - \frac{16e^2 \tan^2\theta}{\beta^2} \tag{6}$$

2.3 Characterization of exothermic reaction

The exothermic reaction characteristics were measured as follows, as shown in Fig. 2. A multilayer powder was placed directly beneath the radiation thermometer, then the current from a DC stabilized power supply was applied to it to generate a microspark. The powder was evenly distributed over a layer of insulating material 1 mm deep and 7 mm in diameter. The focus of the radiant thermometer (1.8 mm in diameter) was adjusted to align with the center of the powder. The spark was generated at the outer edge where the powder was placed. By implementing these precautionary measures during the measurement process, we established conditions under which the temperatures of the materials can be compared on an equivalent basis. At this time, the voltage used for the spark was 20 V and the current was 1 A. Additionally, the data logger's measurement interval was 10 μs. The exothermic reaction behavior was measured using a radiation thermometer over the temperature range of 800–2300 ℃.

2.4 Characterization of heat conduction in microstructure of Al/Ni multilayer

In this study, the thermal properties of the microstructure were measured using a thermal microscope (TM, Bethel Co.) by the TR method, as shown in Fig. 3. The spatial resolution of the probing laser was 1 μm and the modulation frequency of the heating laser was 100 kHz. The principle of the TR method is briefly explained below.[28] A thin metal film was first deposited on the sample surface by sputtering. In the TR method, both the heating and probing laser beams are coaxially focused on the sample surface. The metal film is periodically heated by the heating laser, inducing small temperature oscillations that can be detected through changes in the reflectivity of the metal layer. The surface temperature response is expressed as

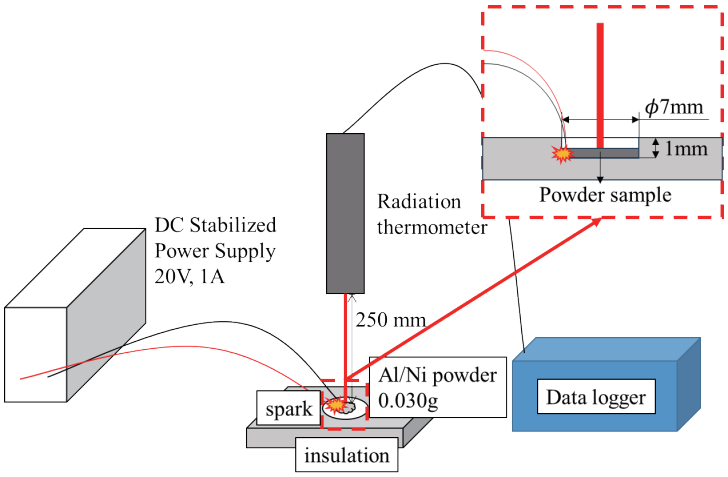

Fig. 2. (Color online) Schematic of exothermic reaction test.

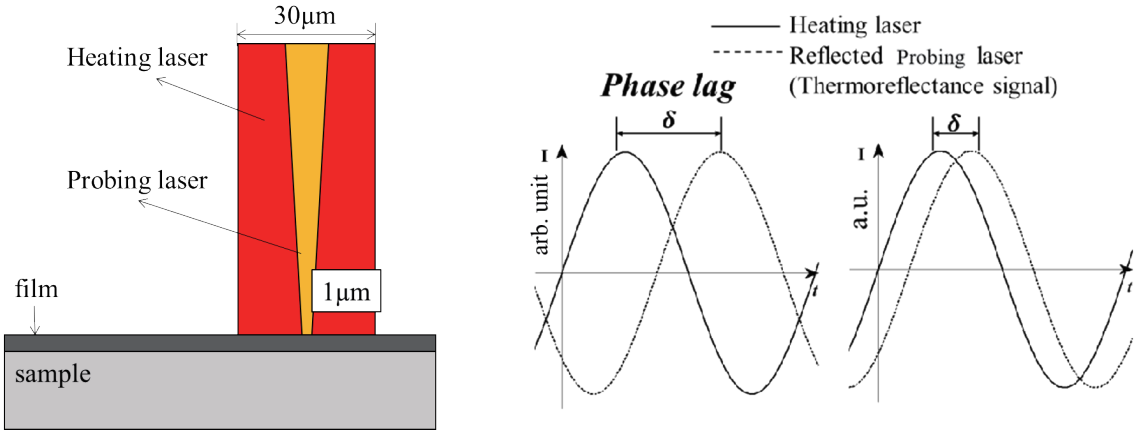

Fig. 3. (Color online) Schematic of TR method.

$$T_1(r,t) = \int_0^\infty \tau_1(p, z=0) J_0(pr)\, p\, dp\, e^{i\omega t} + c.c. \tag{7}$$

The temperature response on the sample surface is denoted as $T_1(r,t)$, which represents the complex temperature oscillation at the radial position r and time t under periodic heating.

$$R(t) = c_{norm} \int_0^\infty T_1(r,t) f_p(r) 2\pi r\, dr \tag{8}$$

The TR signal $R(t)$ is obtained as the convolution of the surface temperature distribution $T_1(r,t)$ with the spatial intensity profile of the probe laser $f_p(r)$.

$$f_p(r) = \left(\frac{P_p}{\pi\sigma_p^2}\right)\exp\left[-\left(\frac{r}{\sigma_p}\right)^2\right] \tag{9}$$

Here, $f_p(r)$ represents the Gaussian intensity distribution of the probe beam with the power P_p and $1/e^2$ radius σ_p. The complex amplitude of $R(t)$ provides both the amplitude A and the phase lag δ of the temperature response, expressed as

$$\delta = Arg\left[R(0)\right], \tag{10}$$

where $Arg\left[R(0)\right]$ denotes the argument (phase angle) of the complex number. The phase lag δ corresponds to the delay between the modulated heating laser and the measured TR signal, and it depends on the thermophysical properties of the Mo thin film and the underlying sample. As the thermal diffusivity of the sample increases, the phase difference between the periodic temperature oscillation at the surface of the metal film and the modulated heating laser becomes smaller. Because the reflectivity of the metal surface varies with temperature, the reflected intensity of the probing laser also changes periodically in synchrony with the temperature modulation. This reflected signal is referred to as the TR signal. The phase difference between the heating laser and the resulting TR signal is defined as the phase lag. Molybdenum (Mo) is commonly selected as a thin-film material because its reflectivity and transmittance are suitable for both the probe laser and the heating laser. In this study, Mo was selected as the thin-film material for cross-sectional measurements of Al/Ni multilayer powders composed of an Al–Ni mixed phase. Furthermore, since the calculation formula assumes a homogeneous single phase, it can explain why phase lag correlates with thermal conductivity. However, since the evaluation region consists of a mixed phase of Al and Ni, conversion to thermal conductivity was intentionally avoided. Instead, the relative difference in thermal conductivity was examined.

The calorific values of the 20-pass and 40-pass rolled powders were measured using an isothermal calorimeter, following the procedures reported in previous studies. An average calorific value of 1364 J/g with a variance of 317 J/g was obtained for the 20-pass rolled samples, while an average calorific value of 1509 J/g with a variance of 83 J/g was obtained for the 40-pass rolled samples. In addition to the average values, attention should also be paid to the variances. The samples with a higher number of rolling passes exhibit not only greater heat generation but also lower variance.

3. Results and Discussion

3.1 Effect of heat treatment on crystallite size

Figure 4 shows the changes in crystallite size observed before and after heat treatment.

For aluminum, a marked increase in crystallite size was observed in the 20-pass and 30-pass

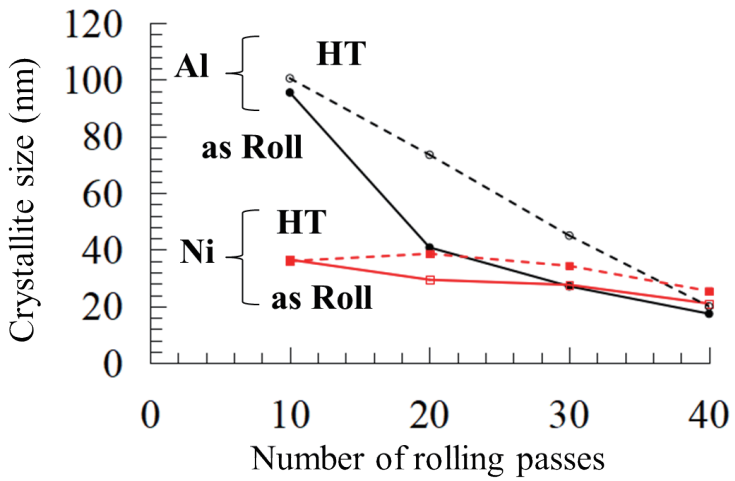

Fig. 4. (Color online) Change in crystallite size per rolling pass.

rolled powders after heat treatment, whereas the 10-pass and 40-pass rolled powders exhibited only a slight increase of approximately 2 nm, showing no significant change overall. A similar tendency was observed for nickel. Although the crystallite size increased by approximately 20–40 nm in the 20-pass and 30-pass rolled powders, no marked change was observed in the other samples. This limited growth in crystallite size is considered to result from the insufficient temperature–time conditions of the annealing treatment, as well as the stored strain energy introduced by severe plastic deformation in both Al and Ni layers. No significant grain growth was observed in either the 10-pass or 40-pass rolled samples. The increase in grain size is generally considered to occur through a mechanism similar to recrystallization, which is a softening process that occurs after recovery and is primarily driven by the release of strain energy accumulated during deformation. This process is powered by the strain energy stored in dislocations generated by plastic deformation. For specimens subjected to relatively low strain, such as those rolled only ten times, the accumulated energy is limited. Consequently, the driving force may be insufficient to overcome the high thermal activation energy required for recrystallization. Conversely, in the 40-pass rolled specimens that experienced severe deformation, the available thermal energy may be insufficient to promote the migration of high-angle grain boundaries (HABs) necessary for recrystallization, since much of the thermal energy is consumed during the recovery process.[25,29,30]

3.2 Effects of heat treatment on exothermic reaction characteristics

Figure 5 shows the temperature variation from the onset of the exothermic reaction (800 °C, corresponding to the lower probing limit of the radiation thermometer) to 0.2 s after initiation for the 30-pass and 40-pass rolled powders. Although slight fluctuations were observed among the measurements, the heat-treated samples exhibited a notable delay in reaction.

Figure 6 indicates the average elapsed time (n = 3) required to reach the target temperature for the highly reactive 30-pass and 40-pass rolled powders. The heat-treated multilayer powders exhibited more than twice the average elapsed time at each temperature compared with the as-

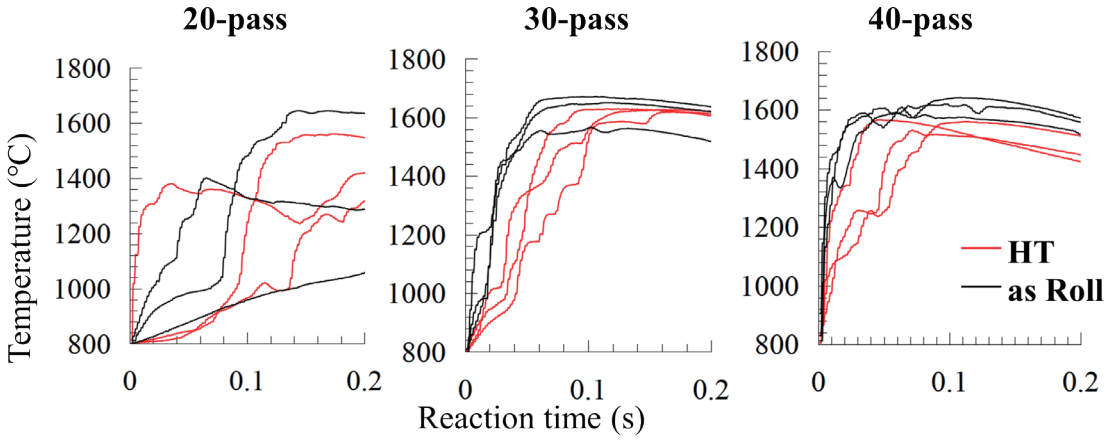

Fig. 5. (Color online) Changes in exothermic reaction characteristics observed before and after heat treatment.

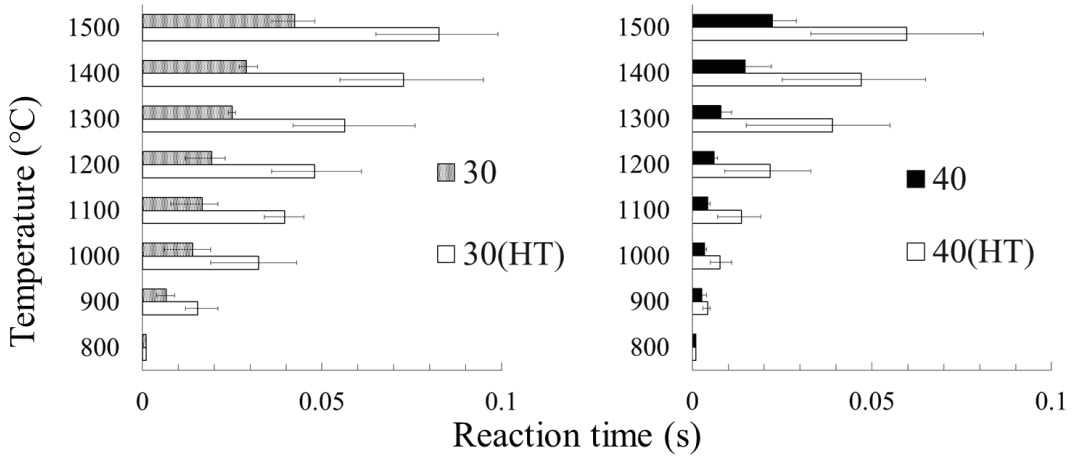

Fig. 6. Average elapsed time required to reach target temperature for the highly reactive 30-pass and 40-pass rolled powders.

rolled powders, indicating that the reaction propagation rate decreased after heat treatment. Furthermore, grain growth was observed in the 20-pass and 30-pass rolled samples, whereas the 40-pass rolled sample exhibited almost no grain growth. However, the reaction propagation rate was found to be higher in the 40-pass rolled powder than in the 20-pass and 30-pass rolled powders.

These results suggest that factors more influential than grain growth affected the exothermic reaction characteristics under the heat treatment conditions employed in this study, and since no significant change in crystallite size was observed while the reaction time was clearly delayed, it is highly likely that an interfacial mixing layer between Al and Ni expanded during heat treatment, similar to that observed in multilayer films, thereby reducing the reaction propagation rate. The exothermic behavior of Al/Ni multilayer materials can be described by the modified heat conduction equation proposed by Gavens *et al.*, which incorporates atomic diffusion perpendicular to the multilayer structure. Gavens *et al.* suggested that the presence of a mixing

layer decreases the available energy for the self-propagating exothermic reaction of Al/Ni, resulting in a lower maximum reaction temperature and a reduction in atomic diffusion driving force, consequently slowing down the reaction. From the results of this experiment, it is considered that Gavens *et al.*'s approach can similarly be applied to multilayer powders.

3.3 Heat conduction in microstructure

The phase lag mapping of the cross sections for the 20-pass and 40-pass rolled powders is shown in Fig. 7.

The measurements were conducted by scanning a 5 × 5 μm^2 area with a 0.5 μm step size. As described above, a smaller phase lag indicates superior thermal transport properties. The results for the 20-pass rolled powder reveal clear differences in thermal transport characteristics between Al and Ni: Al exhibits relatively high thermal conductivity, whereas Ni shows low conductivity. This suggests that the inhomogeneous microstructure of the powder leads to spatially nonuniform thermal transport across the cross section. In contrast, the 40-pass rolled powder shows almost uniform thermal transport properties throughout the cross section. As mentioned above, considering that the spatial resolution of the probing laser is 1 μm, this indicates that heat is transferred uniformly when the heat transfer distance is at least 1 μm. Figure 7 shows the phase delay distribution in the cross section of the powder "before reaction (unreacted state)", not after reaction. This comparison is important for evaluating the effect of the uniformity of local heat transport properties on the stability of self-propagating reactions. In the 20-pass powder, the heat transport properties differ significantly between Al and Ni, with Ni acting as a local heat transport barrier. In contrast, the 40-pass powder exhibits thermal transport homogenization on scales exceeding 1 μm, which is considered to contribute to continuous heat propagation during the reaction and high reaction stability. These findings indicate that, as the cross-sectional structure becomes finer with increasing number of rolling cycles, the thermal transport properties become more uniform. As previously mentioned, the self-propagating exothermic reaction in actual Al/Ni multilayer materials occurs as a chain of instantaneous reactions at the nanoscale and nanosecond timescale, which manifests as a discontinuous self-

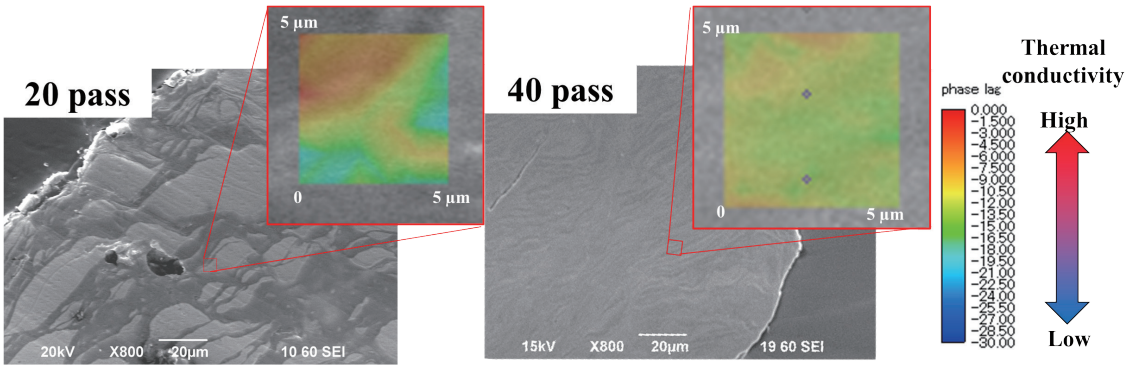

Fig. 7. (Color online) Phase lag distributions in Al/Ni multilayer powder after 20 and 40 passes.

propagating reaction at the macroscale. For a subsequent reaction to propagate from one reactive region to the next, there must be no factors that impede thermal transport between these regions. If any barrier exists during the instantaneous reaction, the continuous reaction is interrupted, resulting in the formation of unreacted regions and a reduction in heat propagation speed.

The present measurements allowed the visualization of the differences in thermal transport characteristics between Al and Ni at the micro- and nanoscales. In the low-pass (20-pass) powders, Ni clearly exhibited lower thermal transport characteristics than Al. This suggests that, in powders with fewer rolling cycles, Ni can impede heat transport during instantaneous reactions, leading to the formation of unreacted regions and a delay in reaction propagation.

4. Conclusions

In this study, heat treatment at 180 °C for 48 h was conducted to evaluate how microstructural changes affect calorific value characteristics. XRD analysis revealed a slight increase in crystallite size for the 20- and 30-pass powders, whereas the 40-pass powder showed almost no change, likely due to insufficient recrystallization at the relatively low temperature. Exothermic measurements demonstrated that the heat-treated powders exhibited a reduced rate of temperature increase rate and approximately twice the reaction completion time compared with untreated powders. Because the change in crystallite size was minimal, the delayed reaction is attributed to the expansion of the Al/Ni interfacial mixing layer during heat treatment, which decreased the diffusion driving force and reaction rate.

Furthermore, TR measurements were employed to evaluate the microscale thermal transport properties of powder cross sections. The results showed a clear difference between Al and Ni in the 20-pass powders, where Ni acted as a local thermal barrier, while the 40-pass powders exhibited uniform phase lag across the cross section, indicating an improved continuity of thermal transport pathways. Since self-propagating exothermic reactions in Al/Ni multilayers proceed as nanoscale, nanosecond chain reactions, such continuous heat transport paths are crucial. These findings demonstrate that, in low-pass powders, Ni regions impede heat transport, causing delayed propagation, whereas high-pass powders possess uniform microstructures that enable stable and rapid heat release.

In summary, the results of this study newly revealed that the exothermic reaction delay under heat treatment conditions cannot be explained by crystallite growth alone, but is closely related to the expansion of the interfacial mixing layer and the local deterioration of thermal transport. Moreover, the TR analysis newly uncovered that Ni regions in low-pass powders act as nanoscale thermal barriers, clarifying the microscopic origin of the reduced reaction rate. On the other hand, in this study, we also identified two remaining challenges. First, because the crystallite size change was limited under the current heat treatment conditions, its effect on reaction behavior could not be fully evaluated. Second, the thickness and composition of the interfacial mixing layer were not quantitatively analyzed. Therefore, future studies should include heat treatments at higher temperatures or with longer durations to enhance crystallite growth and a combination of advanced nanoscale analysis techniques to precisely characterize the interfacial mixing layer and its effect on thermal reaction kinetics.

References

1 J. Wang, E. Besnoin, O. M. Knio, and T. P. Weihs: J. Appl. Phys. **95** (2004) 248. https://doi.org/10.1063/1.1629390
2 J. Wang, E. Besnoin, O. M. Knio, and T. P. Weihs: Acta Mater. **52** (2004) 5265. https://doi.org/10.1016/j.actamat.2004.07.012
3 R. Knepper, M. R. Snyder, G. Fritz, K. Fisher, O. M. Knio, and T. P. Weihs: J. Appl. Phys. **105** (2009) 083504. https://doi.org/10.1063/1.3087490
4 B. Boettge, J. Braeuer, M. Wiemer, M. Petzold, J. Bagdahn, and T. Gessner: J. Micromech: Microeng. **20** (2010) 064018. https://doi.org/10.1088/0960-1317/20/6/064018
5 S. Yamashita, R. Yamamoto, and S. Miyake: Jpn. J Appl. Phys. **60** (2021) SCCL07. https://doi.org/10.35848/1347-4065/abe996
6 S. Miyake, T. Izumi, and R. Yamamoto: Mater. **13** (2020) 4394. https://doi.org/10.3390/ma13194394
7 T. Izumi, N. Kametani, S. Miyake, S. Kanetsuki, and T. Namazu: Jpn. J. Appl. Phys. **57** (2018) 06HJ10. https://doi.org/10.7567/JJAP.57.06HJ10
8 R. Yamamoto, S. Miyake, S. Kanetsuki, T. Namazu, D. Goto, Y. Kuntani, and T. Koganezawa: J. JSEM. **19** (2019) 30. https://doi.org/10.11395/jjsem.19.30
9 T. Namazu, H. Takemoto, H. Fujita, Y. Nagai, and S. Inoue: Proc. 2006 IEEE 19th Micro Electromechanical Systems Conf. (IEEE, 2006) 286. https://doi.org/10.1109/MEMSYS.2006.1627792
10 T. Namazu, K. Ohtani, K. Yoshiki, and S. Inoue: Proc. 2011 16th Int. Solid-State Sensors, Actuators and Microsystems Conf. (2011) 1368. https://doi.org/10.4028/www.scientific.net/MSF.706-709.1979
11 K. Ohtani, Y. Yamano, T. Namazu, and S. Inoue: Proc. Transducers (2009) 172.
12 T. Namazu and S. Inoue: Mater. Sci. Forum. **638**–**642** (2010) 2142. https://doi.org/10.4028/www.scientific.net/MSF.638-642.2142
13 T. Namazu, K. Ohtani, S. Inoue, and S. Miyake: J. Eng. Mater. Technol. **137** (2015) 031011. https://doi.org/10.1115/1.4030413
14 K. Maekawa, S. Ito, and T. Namazu: Jpn. J Appl. Phys. **59** (2020) SIIL01. https://doi.org/10.35848/1347-4065/ab769b
15 S. Miyake, S. Kanetsuki, K. Morino, J. Kuroishi, and T. Namazu: Jpn. J. Appl. Phys. **54** (2015) 06FP15. https://doi.org/10.7567/JJAP.54.06FP15
16 K. Maekawa, K. Kodama, S. Miyake, and T. Namazu: Jpn. J. Appl. Phys. **60** (2021) SCCL15. https://doi.org/10.35848/1347-4065/abf39c
17 S. Yamashita, H. Saegusa, T. Namazu, and S. Miyake: Sens. Mater. **36** (2024) 3433. https://doi.org/10.18494/SAM5163
18 A. S. Ramos, M. T. Vieira, J. Morgiel, J. Grzonka, S. Simoes, and M. F. Vieira: J. Alloys Compd. **484** (2009) 335. https://doi.org/10.1016/j.jallcom.2009.04.098
19 K. Rzyman, Z. Moser, R. E. Watson, and M. Weinert: J. Phase Equilibria **19** (1998) 106. https://doi.org/10.1361/105497198770342562
20 K. Rzyman and Z. Moser: Progress in Mater. Sci. **49** (2004) 581. https://doi.org/10.1016/j.pmatsci.2003.08.001
21 R. Hu, P. Nash, and Q. Chen: J. Phase Equilibria Diffus. **30** (2009) 559. https://doi.org/10.1007/s11669-009-9573-3
22 F. Z. Chrifi-Alaoui, M. Nassik, K. Mahdouk, and J. C. Gachon: J. Alloys Compd. **364** (2004) 121. https://doi.org/10.1016/S0925-8388(03)00493-6
23 A. J. Gavens, D. Van Heerden, A. B. Mann, M. E. Reiss, and T. P. Weihs: J. Appl. Phys. **87** (2000), 1255. http://dx.doi.org/10.1063/1.372005
24 R. Armstrong and M. Koszykowski, in Combustion and Plasma Synthesis of High-Temperature Materials, Z. A. Munir and J. B. Holt, Eds.(VCH, New York, 1990) p. 88.
25 S. Bunkholt, E. Nes, and K. Marthinsen: Metals **9** (2019) 1032. https://doi.org/10.3390/met9101032
26 W. H. Hall: Proc. Phys. Soc. A **62** (1949) 741. https://doi.org/10.1088/0370-1298/62/11/110
27 N. C. Halder and C. N. J. Wagner: Acta Cryst. **20** (1966) 312. https://doi.org/10.1107/S0365110X66000628
28 S. Miyake, G. Matsui, H.i Ohta, K. Hatori, K. Taguchi and S.Yamamoto: Meas. Sci. Technol. **28** (2017) 075006 (7pp). https://doi.org/10.1088/1361-6501/aa72d0
29 O. V. Mishin, A. Godfrey, D. Juul Jensen, and N. Hansen: Acta Mater. **61** (2013) 5354. https://doi.org/10.1016/j.actamat.2013.05.024
30 Z. Li, Y. Wu, Z. Xie, C. Kong, and H. Yu: Mater. **14** (2021) 4025. https://doi.org/10.3390/ma14144025